*inorganics*

MDPI

*Article*

# The Structures and Bonding of Bismuth-Doped Boron Clusters: $BiB_4^-$ and $BiB_5^-$

**Hyun Wook Choi, Wei-Jia Chen, G. Stephen Kocheril, Dao-Fu Yuan * and Lai-Sheng Wang ***

Department of Chemistry, Brown University, 324 Brook Street, Providence, RI 02912, USA
* Correspondence: ydfu@ustc.edu.cn (D.-F.Y.); lai-sheng_wang@brown.edu (L.-S.W.)

**Abstract:** We present an investigation on the structures and chemical bonding of two Bi-doped boron clusters $BiB_n^-$ ($n$ = 4, 5) using photoelectron spectroscopy and theoretical calculations. The electron affinities of $BiB_4$ and $BiB_5$ are measured to be 2.22(2) eV and 2.61(2) eV, respectively. Well-resolved photoelectron spectra are obtained and used to compare with theoretical calculations to verify the structures of $BiB_4^-$ and $BiB_5^-$. Both clusters adopt planar structures with the Bi atom bonded to the periphery of the planar $B_n$ moiety. Chemical bonding analyses reveal that the $B_n$ moiety maintains σ and π double-aromaticity. The Bi atom is found to induce relatively small structural changes to the $B_n$ moiety, very different from transition metal-doped boron clusters.

**Keywords:** photoelectron spectroscopy; metal boron clusters; bismuth; chemical bonding; planar clusters

check for updates

**Citation:** Choi, H.W.; Chen, W.-J.; Kocheril, G.S.; Yuan, D.-F.; Wang, L.-S. The Structures and Bonding of Bismuth-Doped Boron Clusters: $BiB_4^-$ and $BiB_5^-$. *Inorganics* **2023**, *11*, 405. https://doi.org/10.3390/inorganics11100405

Academic Editors: Jean-François Halet and Gilles Alcaraz

Received: 24 September 2023
Revised: 12 October 2023
Accepted: 12 October 2023
Published: 14 October 2023



## 1. Introduction

Due to its electron deficiency, boron exhibits a wide range of bulk allotropes and compounds that consist of distinct three-dimensional (3D) building blocks [1–3]. Extensive research has been conducted over the past two decades, employing a combination of experimental and theoretical studies to investigate size-selected boron clusters [4–7]. Unlike their bulk counterparts, small boron clusters predominantly exhibit two-dimensional (2D) structures composed mainly of $B_3$ triangles. Among the fascinating 2D boron clusters, the $C_{6v}$ $B_{36}$ cluster stands out as it provides the first experimental evidence for the existence of atom-thin 2D boron (borophene) [8]. Borophenes have been successfully synthesized on metal substrates [9,10], becoming a novel type of synthetic 2D material [11,12]. Another important boron cluster is $B_{40}$, which was found to have a cage structure, the first all-boron fullerene (borospherene) [13]. Numerous boron clusters doped with metals have also been generated and investigated [6,14–16], significantly extending the range of nanostructures that can be formed by boron.

After the discovery of ultrahigh thermal conductivity and important electronic properties in the cubic boron arsenide [17–19], the group III–V semiconductor families have gained increasing attention. However, arsenic compounds come with a significant drawback of toxicity [20,21]. On the other hand, bismuth, the heaviest group V element, is considered to be a "green metal" due to its low toxicity [22] and has attracted interest in chemistry and material sciences [23–25]. There is also growing interest in bismuth boride [26–28], but it has not yet been fabricated thus far. Small Bi boride clusters are ideal models to investigate the bonding between bismuth and boron, which lays the foundation to understand the bulk material and may help discover new Bi-B nanostructures.

Toward this goal, we have studied several Bi-B binary clusters using photoelectron spectroscopy (PES) and theoretical calculations, including $BiB_n^-$ ($n$ = 6–8) [29] and several di-bismuth boride clusters $Bi_2B_n^-$ ($n$ = 1–4) [30,31]. Most recently, we have reported an investigation of cold diatomic $BiB^-$ using high-resolution photoelectron imaging [32]. In the current article, we present a study on the structures and chemical bonding of two Bi-doped boron clusters, $BiB_n^-$ ($n$ = 4, 5), using PES and theoretical calculations. Well-resolved

photoelectron spectra are measured and interpreted using the theoretical results. Both the $BiB_4^-$ and $BiB_5^-$ clusters are found to exhibit 2D structures. The Bi atom is found to be bonded to the edge of $B_4$ and $B_5$, respectively. The Bi atom is observed to induce relatively small structural changes to the $B_n$ motif in comparison to the bare $B_n$ clusters, in contrast to transition metal-doped boron clusters.

## 2. Experimental and Theoretical Methods

### *2.1. Photoelectron Spectroscopy*

The experiments were conducted with a magnetic-bottle PES apparatus. Details of the experimental apparatus and procedures can be found elsewhere [5] and only essential features pertaining to this work are given here. The Bi-doped boron clusters were generated by laser ablation of a disk target made of Bi and $^{10}$B-enriched boron powders (1/1 Bi/B molar ratio). The plasma induced by the vaporization laser was quenched by a high-pressure He carrier gas containing 5% Ar. Clusters from the nozzle were carried by the carrier gas and cooled via supersonic expansion. Anionic clusters in the beam were extracted into a time-of-flight mass analyzer for mass analyses and cluster size selection. The $BiB_n^-$ ($n$ = 4, 5) clusters were each selected by a mass gate and decelerated before crossing a photodetachment laser beam. Three laser wavelengths were used for photodetachment, including 355 nm (3.496 eV) and 266 nm (4.661 eV) from a Nd:YAG laser and 193 nm (6.424 eV) from an ArF excimer laser. Photoelectrons were analyzed in a 3.5 m long electron time-of-flight tube of the magnetic-bottle PES spectrometer. Photoelectron spectra were calibrated with the known transitions of the $Bi^-$ atomic anion. The electron kinetic energy ($E_k$) resolution ($\Delta E_k/E_k$) of the magnetic-bottle analyzer was approximately 2.5%, i.e., about 25 meV for 1 eV electrons.

### *2.2. Theoretical Methods*

Theoretical calculations were carried out to understand the structures and bonding of $BiB_n^-$ ($n$ = 4, 5) and help interpret the photoelectron spectra using the Gaussian 09 program packages [33]. Based on our prior experience [29,31], the Bi atoms tend to bond to the periphery of planar boron cluster motifs. Thus, the Bi atom was put around the planar $B_4$ and $B_5$ motifs [5,6], respectively, for the initial structural searches of $BiB_4^-$ and $BiB_5^-$ at the PBE/aug-cc-pVDZ-pp level. The low-lying isomers were reoptimized at the PBE level using the aug-cc-pVTZ basis set for B and the aug-cc-pVTZ-pp basis set with the relativistic pseudopotentials (ECP60MDF) for Bi [34–36]. We computed the adiabatic detachment energy (ADE) as the energy difference between the anion and the corresponding neutral at their optimized structures. The first vertical detachment energy ($VDE_1$) was calculated as the energy difference between the anion and neutral at the optimized geometry of the anion. Higher VDEs were calculated using time-dependent DFT (TD-DFT) calculations at the PBE/aug-cc-pVTZ level of theory at the anion geometry [37,38]. Although spin–orbit coupling effects were not treated explicitly, we have found that the computed ADEs and VDEs in general agree well with the experimental data. We have also tried the calculations using other functionals, including TPSSH, B3LYP, and PBE0. The results are similar, though the PBE results give a better fit to the experiment.

The chemical bonding of $BiB_n^{-/0}$ ($n$ = 4, 5) was analyzed with the adaptive natural density partitioning (AdNDP) method [39,40]. The AdNDP method has been proven to be an effective tool for understanding the bonding in boron and metal-doped boron clusters. All the AdNDP calculations were carried out with the multiwfn program [41].

## 3. Results

### *3.1. Experimental Results*

The photoelectron spectra of $BiB_4^-$ and $BiB_5^-$ are shown in Figures 1 and 2, respectively, at three photon energies. Detachment transitions are labeled with letters, where X refers to detachment transition from the ground electronic state of the anion to that of the corresponding neutral. The detachment bands labeled from A to D for $BiB_4^-$ and A to G

for $BiB_5^-$ represent transitions from the ground state of the anion to excited states of the neutral final states.

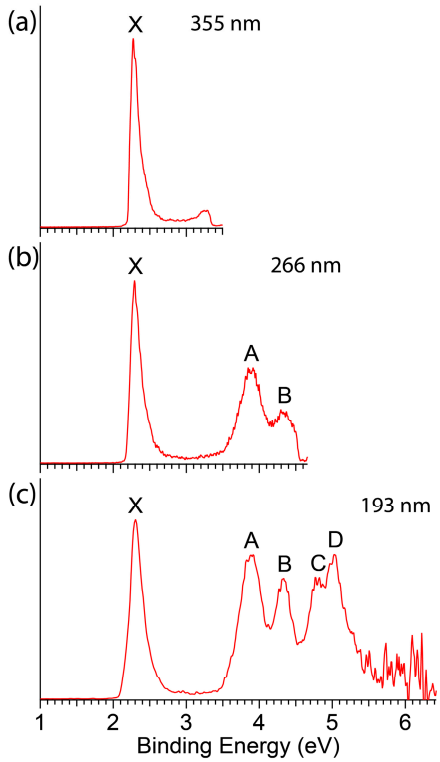


**Figure 1.** Photoelectron spectra of $BiB_4^-$ at (**a**) 355 nm (3.496 eV), (**b**) 266 nm (4.661 eV), and (**c**) 193 nm (6.424 eV).

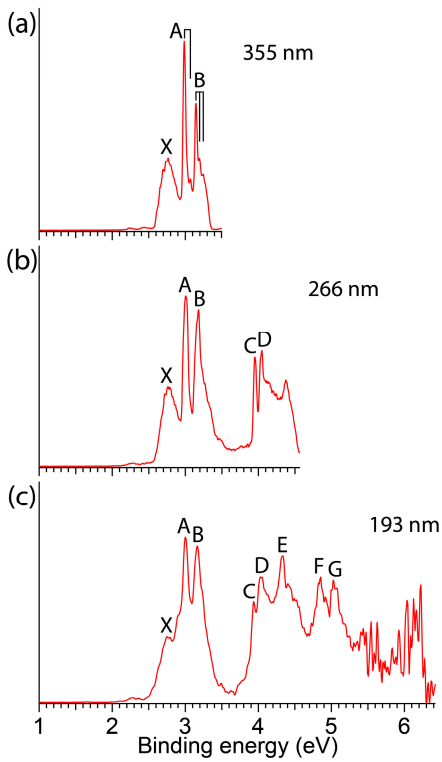


**Figure 2.** Photoelectron spectra of $BiB_5^-$ at (**a**) 355 nm (3.496 eV), (**b**) 266 nm (4.661 eV), and (**c**) 193 nm (6.424 eV).

The photoelectron spectra of $BiB_4^-$ display a relatively simple spectral pattern with well-resolved detachment transitions (Figure 1). The first VDE of $BiB_4^-$ is obtained from band X as 2.27 eV in Figure 1a. The ADE obtained from the onset of band X is 2.22 eV, which also represents the electron affinity (EA) of neutral $BiB_4$. The ADE is estimated by drawing a straight line along the leading edge of band X and then adding the spectral resolution to the intersection with the binding energy axis. There is a large energy gap between band X and the broad band A at a VDE of 3.88 eV. Band B is slightly cut off at 266 nm (Figure 1b) but fully observed in the 193 nm spectrum (Figure 1c) at a VDE of 4.31 eV. Two closely spaced bands, C and D, are observed at VDEs of 4.71 eV and 4.96 eV, respectively. No other detachment transitions are observed at higher binding energies. The ADE and all the VDEs are given in Table 1, where they are compared with the theoretical results.

**Table 1.** The experimental adiabatic (ADE) and vertical (VDE) detachment energy for $BiB_4^-$ in comparison with the calculated values at the PBE/aug-cc-pVTZ level for the GM $C_1$ ($^1$A) structure (Figure 3a). All energies are in eV.

| | VDE/ADE (exp) [a] | Final State and Electron Configuration | VDE/ADE (theo) |
|---|---|---|---|
| X | 2.27/2.22 | $^2$A {...(18a)$^2$(19a)$^2$(20a)$^2$(21a)$^2$(**22a**)$^1$} | 2.16/2.11 |
| A | 3.88 | $^2$A {...(18a)$^2$(19a)$^2$(20a)$^2$(**21a**)$^1$(22a)$^2$} | 3.68 |
| B | 4.31 | $^2$A {...(18a)$^2$(19a)$^2$(**20a**)$^1$(21a)$^2$(22a)$^2$} | 4.10 |
| C | 4.77 | $^2$A {...(18a)$^2$(**19a**)$^1$(20a)$^2$(21a)$^2$(22a)$^2$} | 4.71 |
| D | 4.97 | $^2$A {...(**18a**)$^1$(19a)$^2$(20a)$^2$(21a)$^2$(22a)$^2$} | 4.96 |

[a] The experimental uncertainties are ±0.02 eV.

The photoelectron spectra of $BiB_5^-$ (Figure 2) exhibit more complicated and congested spectral features due to its open-shell electronic structure. At 355 nm (Figure 2a), three closely spaced detachment transitions (X, A, B) are observed. The broader band X at a VDE of 2.74 eV should represent the transition from the ground electronic state of $BiB_5^-$ to that of neutral $BiB_5$. The ADE is estimated from band X to be 2.61 eV, i.e., the EA of $BiB_5$. The A and B bands at VDEs of 2.99 and 3.15 eV, respectively, are sharp with partially resolved vibrational structures. The vibrational spacings for bands A and B are estimated to be 640 and 400 cm$^{-1}$, respectively. Following an energy gap, a series of congested detachment transitions (C to G) are observed above 4 eV. Bands C and D at 3.95 and 4.05 eV, respectively, are very closely spaced and are shown to be quite sharp at 266 nm (Figure 2b). The 193 nm spectrum reveals three more bands, E, F, and G, at 4.33, 4.86, and 5.02 eV, respectively (Figure 2c). The signal-to-noise ratios are too poor above 5 eV in the 193 nm for definitive identification of more detachment features. The ADE and all VDEs for $BiB_5^-$ are given in Table 2, where they are compared with the theoretical results.

**Table 2.** The experimental adiabatic (ADE) and vertical detachment energy (VDE) for $BiB_5^-$ in comparison with the calculated values at the PBE/aug-cc-pVTZ level for the GM $C_s$ ($^2$A′) structure (Figure 4a). All energies are in eV.

| | VDE/ADE (exp) [a] | Final State and Electron Configuration | VDE/ADE (theo) |
|---|---|---|---|
| X | 2.74/2.61 | $^1$A′ {...(17a′)$^2$(18a′)$^2$(19a′)$^2$(5a″)$^2$(**20a′**)$^0$} | 2.92/2.70 |
| A | 2.99 | $^3$A″ {...(17a′)$^2$(18a′)$^2$(19a′)$^2$(**5a″**)$^1$(20a′)$^1$} | 2.93 |
| B | 3.15 | $^1$A″ {...(17a′)$^2$(18a′)$^2$(19a′)$^2$(**5a″**)$^1$(20a′)$^1$} | 3.25 |
| C | 3.95 | $^3$A′ {...(17a′)$^2$(18a′)$^2$(**19a′**)$^1$(5a″)$^2$(20a′)$^1$} | 3.85 |
| D | 4.05 | $^3$A′ {...(17a′)$^2$(**18a′**)$^1$(19a′)$^2$(5a″)$^2$(20a′)$^1$} | 3.99 |
| E | 4.33 | $^1$A′ {...(17a′)$^2$(18a′)$^2$(**19a′**)$^1$(5a″)$^2$(20a′)$^1$} | 4.43 |
| | | $^3$A′ {...(**17a′**)$^1$(18a′)$^2$(19a′)$^2$(5a″)$^2$(20a′)$^1$} | 4.63 |
| F | 4.86 | $^1$A′ {...(17a′)$^2$(**18a′**)$^1$(19a′)$^2$(5a″)$^2$(20a′)$^1$} | 5.03 |
| G | 5.02 | $^1$A′ {...(**17a′**)$^1$(18a′)$^2$(19a′)$^2$(5a″)$^2$(20a′)$^1$} | 5.15 |

[a] The experimental uncertainties are ±0.02 eV.

### 3.2. Theoretical Results

The global minima and low-lying isomers for $BiB_4^-$ and $BiB_5^-$ are displayed in Figures 3 and 4, respectively, as well as the corresponding neutral structures. The global minimum of $BiB_4^-$ (GM, Figure 3a) was found to be closed-shell ($^1$A) with a quasi-planar structure ($C_1$ symmetry) at the PBE level of theory. The $B_4$ motif of $BiB_4^-$ is similar to the global minimum of the bare $B_4$ cluster. In fact, the Bi atom can be viewed as replacing a B atom in $B_5^-$, which has a planar $C_{2v}$ structure. A 3D isomer is located for $BiB_4^-$, which is 1.30 eV above the GM structure (Iso1, Figure 3a).

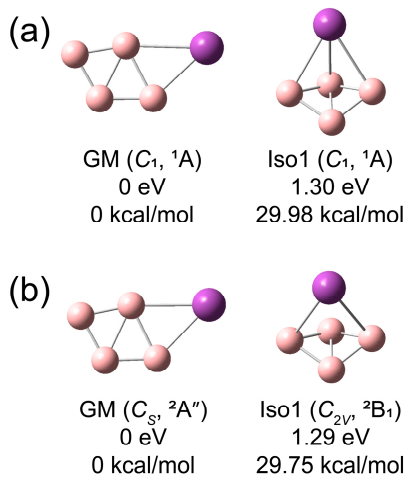


**Figure 3.** The global minima and a low-lying isomer of (**a**) $BiB_4^-$ and (**b**) $BiB_4$. Relative energies are given in eV and kcal/mol at the PBE/aug-cc-pVTZ level.

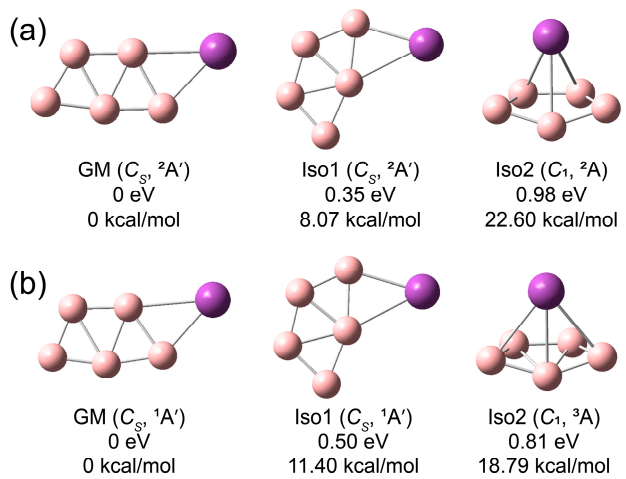


**Figure 4.** The global minima and low-lying isomers of (**a**) $BiB_5^-$ and (**b**) $BiB_5$. Relative energies are given in eV and kcal/mol at the PBE/aug-cc-pVTZ level.

The neutral ground state (Figure 3b) is similar to that of the anion, except that it is planar with a doublet spin state ($C_s$, $^2$A″). The low-lying isomer of neutral $BiB_4$ (Iso1, Figure 3b) is also similar to that of the anion, but it is more symmetric with $C_{2v}$ symmetry. The large energy difference between Iso1 and the GM structure of the anion is maintained in the neutral system. The computed ADE and VDEs for the global minimum of $BiB_4^-$ are compared with the experimental results in Table 1.

The global minimum of $BiB_5^-$ (GM, Figure 4a) has a planar structure with a doublet spin state ($C_s$, $^2$A′). The Bi atom is bonded to the edge of a planar $B_5$ motif, which is similar to the bare $B_5$. In fact, the GM of $BiB_5^-$ is similar to that of neutral $B_6$ and the Bi atom can be viewed as substituting an apex B atom of the planar $B_6$. The next low-lying isomer of

$BiB_5^-$ is 0.35 eV higher in energy than the GM structure at the PBE level, Iso1 ($C_s$, $^2A'$) in Figure 4a. The $B_5$ motif in Iso1 of $BiB_5^-$ is similar to that in the GM structure, but the position of the Bi atom is different. The second low-lying isomer (Iso2, Figure 4a) is a 3D structure, being 0.98 eV higher in energy than the GM structure. In Iso2, the Bi atom is located above a pentagonal $B_5$ motif with $C_1$ symmetry ($^2A$). The triangular isomer with the Bi atom at one of the apexes is also found, but it is much higher in energy (1.78 eV above the GM). The neutral $BiB_5$ GM and its low-lying isomers (Figure 4b) are similar to the anion with the same energy ordering. The computed ADE and VDEs for the GM of $BiB_5^-$ are given in Table 2, where they are compared with the experimental results.

## 4. Discussion

### *4.1. Comparison between Experiment and Theory*

The experimental PES data are essential for verifying the global minima of $BiB_4^-$ and $BiB_5^-$. The assignments of the experimental PES features are presented in Tables 1 and 2 for $BiB_4^-$ and $BiB_5^-$, respectively, according to the computed VDEs for the global minimum of each cluster. The theoretical VDEs are also given as vertical bars under the 193 nm spectra in Figures 5 and 6 for $BiB_4^-$ and $BiB_5^-$, respectively. The valence molecular orbitals are presented in Figures S1 and S2 for $BiB_4^-$ and $BiB_5^-$, respectively.

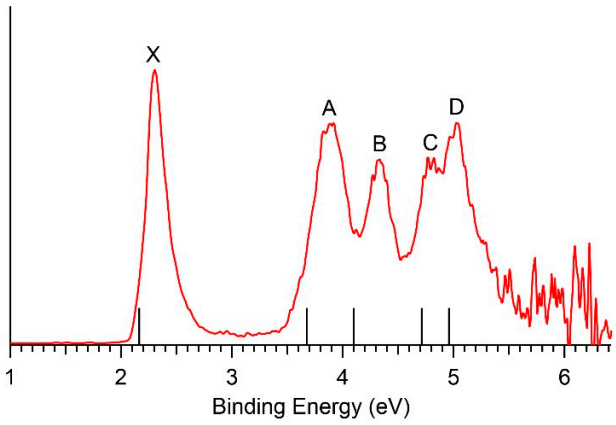


**Figure 5.** Comparison of the computed VDEs with the photoelectron spectrum of $BiB_4^-$ at 193 nm. The vertical bars correspond to computed VDEs at the PBE/aug-cc-pVTZ level of theory.

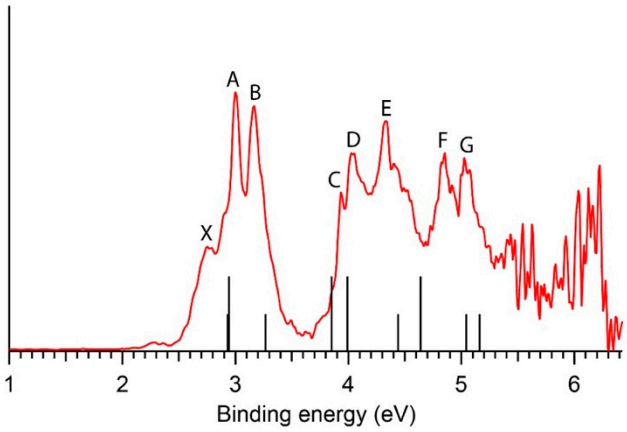


**Figure 6.** Comparison of the computed VDEs with the photoelectron spectrum of $BiB_5^-$ at 193 nm. The vertical bars correspond to computed VDEs at the PBE/aug-cc-pVTZ level of theory. The longer and shorter bars correspond to transitions to triplet and singlet final states, respectively.

#### 4.1.1. $BiB_4^-$

The computed $VDE_1$/ADE of 2.16/2.11 eV for the GM structure of $BiB_4^-$ at the PBE level agree well with the measured values of 2.27/2.22 eV (Table 1). Even though the isomer Iso1 also gives similar computed $VDE_1$/ADE values (2.34/2.10 eV), its energy is higher than the GM structure by 1.30 eV. Thus, it can be ruled out from any contributions to the experimental spectra. In addition, the large difference between the computed $VDE_1$ and ADE of Iso1, due to the significant geometry change between its neutral and anion (Figure 3), would suggest a broad detachment transition, which is inconsistent with the relatively sharp band X in the spectra of $BiB_4^-$ (Figure 1). The calculated VDE for higher binding energy detachment channels of the $C_1$ global minimum are compared with the experimental data in Table 1 and in Figure 5 as the vertical bars.

The first detachment channel is from the HOMO (22a), a π-type MO primarily of Bi $6p_z$ character with a small contribution from the $B_4$ moiety (Figure S1). The electron detachment from the HOMO leads to a geometry change from the quasi-planar structure ($C_1$) to the planar neutral $BiB_4$ ($C_s$) (Figure 3). The narrow width of band X agrees with the small structural change between the ground state of the anion and that of the neutral (Figure S3a). Electron detachment from the HOMO-1 (21a) gives a computed VDE of 3.68 eV, which agrees well with the measured VDE of band A at 3.88 eV. The HOMO-1 is an in-plane σ-type MO, involved in B–B bonding and Bi–B bonding (Figure S1). The bonding nature of the HOMO-1 is consistent with the relatively broad band A. Electron detachment from the HOMO-2 (20a) results in a theoretical VDE of 4.10 eV, in good agreement with the measured VDE of band B at 4.31 eV. The 20a orbital is also an in-plane σ-type MO, involved in B–B bonding and Bi–B bonding (Figure S1). The HOMO-3 (19a) and HOMO-4 (18a) are an in-plane σ MO and a π MO, respectively (Figure S1). The calculated VDEs from these orbitals (4.71 eV and 4.96 eV) also match well with the measured VDEs of band C (4.77 eV) and band D (4.97 eV), respectively. The closed-shell GM structure of $BiB_4^-$ is responsible for its relatively simple photoelectron spectra. The computed VDEs are in good agreement with the observed spectral pattern (Figure 5), providing strong support for the quasi-planar $C_1$ GM structure of $BiB_4^-$.

#### 4.1.2. $BiB_5^-$

The computed $VDE_1$/ADE for the global minimum of $BiB_5^-$ are 2.92/2.70 eV at the PBE level (Table 2). The computed ADE agrees well with the measured value of 2.61 eV, though the theoretical VDE is overestimated by 0.18 eV compared to the experimental VDE of 2.74 eV. The larger theoretical discrepancy is probably due to the open-shell nature of $BiB_5^-$. The computed $VDE_1$ of 2.79 eV and 2.64 for Iso1 and Iso2, respectively, at the PBE level are lower than that for the GM structure (Table S1). Very weak signals are observed on the lower binding energy side of band X. They could come from contributions of these higher-energy isomers, but their contributions to the main spectral features should be negligible. The computed VDEs for higher binding energy detachment channels of the GM structure of $BiB_5^-$ are presented in Table 2 and in Figure 6 as vertical bars. Both singlet and triplet final states are possible for detachment from the open-shell GM of $BiB_5^-$ (Figure 4a). The longer bars in Figure 6 represent triplet final states and the shorter bars represent singlet final states.

Although both the GM structures of $BiB_5^-$ and neutral $BiB_5$ are planar with $C_s$ symmetry, there are significant bond length changes (Figure S3b), in accordance with the broad band X. The first detachment channel is from the 20a′ SOMO of $BiB_5^-$, which is an in-plane σ-type orbital (Figure S2). The next detachment channel is from the HOMO (5a″), resulting in a high-spin ($^3A''$) and a low-spin ($^1A''$) final state. The computed VDEs for the triplet and singlet final states, 2.93 eV and 3.25 eV (Table 2), agree well with the experimental observation for band A (2.99 eV) and band B (3.15 eV), respectively. Detachment from the HOMO-1 (19a′) similarly gives rise to a triplet ($^3A'$) and a singlet ($^1A'$) neutral state.

The calculated VDE for the $^3A'$ triplet state (3.85 eV) is consistent with band C at 3.95 eV, whereas that for the singlet $^1A'$ final state (4.43 eV) is consistent with band E at 4.33 eV. Detachment from the HOMO-2 (18a′) gives a high-spin final state ($^3A'$) with a computed VDE of 3.99 eV and a low-spin ($^1A'$) final state with a computed VDE of 5.03 eV,

in good agreement with band D at 4.05 eV and F at 4.86 eV, respectively. Finally, detachment from the HOMO-3 (17a′) leads to a triplet final state ($^3$A′) with a computed VDE of 4.63 eV and a singlet final state ($^1$A′) with a computed VDE of 5.15 eV. Band E has a broad shoulder on the high binding energy side (not labeled), which agrees with the computed VDE of the triplet final state of the 17a′ HOMO-3, whereas the singlet final state is assigned to band G at 5.02 eV. The open-shell nature of $BiB_5^-$ results in the congested spectral features, making their definitive assignment rather challenging. Nevertheless, the overall spectral pattern from the computed VDEs is in reasonable agreement with the experiment, as shown in Figure 6, providing credence for the $C_s$ GM structure of $BiB_5^-$.

### *4.2. Chemical Bonding in the Bismuth–Boron Clusters*

To gain insights into the structures and bonding of the $BiB_4^-$ and $BiB_5^-$ clusters, we conducted AdNDP analyses, as depicted in Figures 7 and 8, respectively. The $6s^2$ electrons of the Bi atom are strongly stabilized due to the relativistic effects [42], rendering them less active in chemical bonding. Consequently, chemical bonding in Bi compounds primarily involves the $6p$ orbitals with little $sp$ hybridization. The $6s^2$ electrons remain as a lone pair in all bismuth–boron clusters [29–32]. Similarly, we find a $6s^2$ lone pair in the current bismuth–boron clusters, whereas the $6p_x$ and $6p_y$ orbitals participate in σ-bonding with the $B_n$ moiety and the $6p_z$ orbital engages in π-bonding with the $B_n$ moiety. Because of the large size of the Bi atom and the strong B–B bonds, it is not favorable for the Bi atom to insert into the $B_n$ moiety. Thus, in both $BiB_4^-$ and $BiB_5^-$ we find that the Bi atom is bonded to the edge of the planar $B_n$ moiety, similar to other binary Bi-B clusters [29,31].

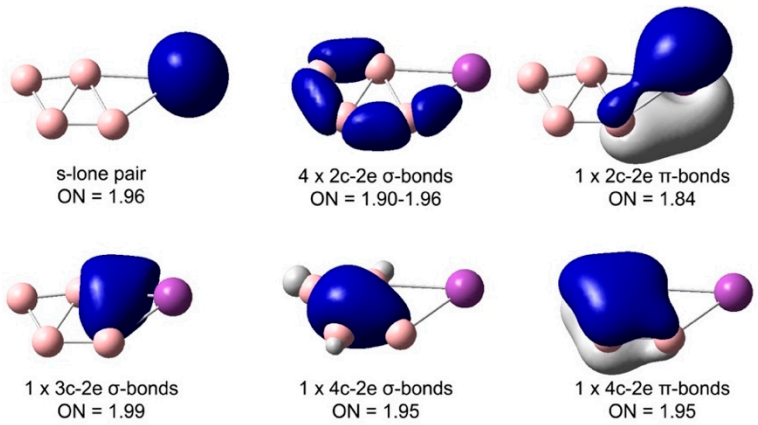


**Figure 7.** AdNDP bonding analysis for the global minimum structure of $BiB_4^-$. ON stands for occupation number.

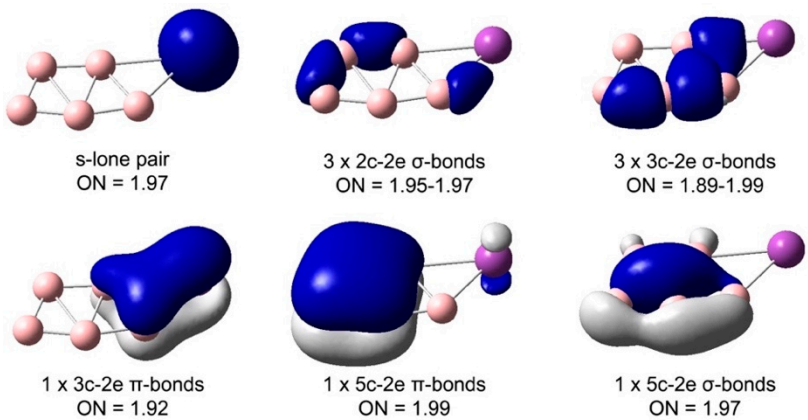


**Figure 8.** AdNDP bonding analysis for the global minimum structure of $BiB_5$. ON stands for occupation number.

In addition to the 6*s* lone pair, the AdNDP analysis for $BiB_4^-$ (Figure 7) reveals four two-center two-electron (2c-2e) σ-bonds (three B–B bonds and one Bi–B bond) on the edge of the quasi-planar $BiB_4^-$ cluster, one 2c-2e Bi–B π-bond, one delocalized 3c-2e σ-bond ($BiB_2$), one delocalized 4c-2e σ-bond, and one delocalized 4c-2e π-bond on the $B_4$ moiety. Each of the delocalized 4c-2e σ- and π-bonds satisfies the $4N + 2$ Hückel rule for aromaticity, rendering the $B_4$ moiety doubly aromatic, similar to the doubly aromatic bare $B_4$ cluster [43]. Thus, the $BiB_4^-$ cluster can be considered as Bi bridge-bonded to a doubly aromatic $B_4$ cluster. It should be noted that the Bi atom has two different Bi–B bonds (2.20 and 2.41 Å) in $BiB_4^-$ (Figure S3a). The shorter Bi–B bond is similar to a Bi=B double bond according to Pyykkö's self-consistent atomic covalent radii of B and Bi (2.19 Å) [44].

The double Bi=B bond is borne out by the AdNDP analysis (Figure 7), where a 2c-2e Bi–B σ-bond and a 2c-2e Bi–B π-bond are clearly seen. The longer Bi–B bond in $BiB_4^-$ is actually weaker than a single Bi–B bond (2.36 Å according to Pyykkö's covalent atomic radii), because the longer Bi–B bond is involved in the delocalized 3c-2e σ-bond. The Bi atom induces relatively small structural changes to the $B_4$ moiety compared to the bare $B_4$. This bonding situation is very different from transition metal $MB_4$ clusters [16], where the strong M–B bonding can completely change the $B_4$ moiety relative to the bare $B_4$. For example, the $ReB_4^-$ cluster has a pentagonal structure and displays Möbius aromaticity due to the strong participation of the Re 4*d* orbitals in chemical bonding with boron [45,46].

For $BiB_5^-$, we chose to conduct the AdNDP analysis on the closed-shell $BiB_5$ neutral for convenience, as shown in Figure 8. The AdNDP results reveal the expected 6*s* lone pair on Bi, three 2c-2e σ-bonds (two B–B bonds and one Bi–B bond) on the periphery of the planar $BiB_5$ cluster, three delocalized 3c-2e σ-bonds (two over two $B_3$ units and one over the $BiB_2$ unit), one delocalized 3c-2e π-bond over the $BiB_2$ unit, one delocalized 5c-2e π-bond, and one delocalized 5c-2e σ-bond over the $B_5$ moiety. The delocalized σ- and π-bonds over the $B_5$ moiety render it doubly aromatic, similar to the bare $B_5$ cluster [43]. Thus, $BiB_5$ can be viewed as a Bi atom bridge-bonded to the periphery of the $B_5$ moiety. The two Bi–B bonds in $BiB_5$ are also asymmetric, similar to those in $BiB_4^-$. Again, the Bi atom in $BiB_5$ induces relatively small changes in the $B_5$ moiety in comparison to the bare $B_5$ cluster, very different from transition metal $MB_5$ clusters [26]. For example, the $TaB_5$ cluster has a fan-shaped structure, in which the Ta atom is bonded to all five B atoms. We found that the larger $BiB_n^-$ ($n$ = 6–8) clusters behave similarly [29], in that their GM structures can be viewed as Bi bonded to the edge of the planar $B_n^-$ clusters, respectively.

## 5. Conclusions

In conclusion, we report an investigation of the structures and bonding of two Bi-doped boron clusters, $BiB_4^-$ and $BiB_5^-$, using photoelectron spectroscopy. Well-resolved photoelectron spectra are obtained and interpreted using theoretical calculations. Electron affinities of $BiB_4$ and $BiB_5$ are measured to be 2.22(2) eV and 2.61(2) eV, respectively, and the experimental vertical detachment energies are compared with theoretical calculations to verify the structures of $BiB_4^-$ and $BiB_5^-$. The $BiB_4^-$ cluster is found to be quasi-planar with $C_1$ symmetry ($^1$A), whereas $BiB_5^-$ is found to be planar with $C_s$ symmetry ($^2$A′). Chemical bond analyses show that the Bi atom is bridge-bonded on the periphery of the respective $B_n$ clusters with relatively small structural change relative to the bare $B_n$ clusters. The two Bi–B bonds in the two clusters are asymmetric with a Bi=B double bond and a weak Bi–B single bond in both clusters.

**Supplementary Materials:** The following supporting information can be downloaded at: https://www.mdpi.com/article/10.3390/inorganics11100405/s1. Figure S1. The valence MOs of the global minimum of $BiB_4^-$ ($C_1$, $^1$A). Figure S2. The valence MOs of the global minimum of $BiB_5^-$ ($C_s$, $^2$A′). Figure S3. The bond lengths (in Å) for (a) the ground state of $BiB_4^-$ ($C_1$, $^1$A) and $BiB_4$ ($C_s$, $^2$A″) and (b) the ground state of $BiB_5^-$ ($C_s$, $^2$A′) and $BiB_5^-$ ($C_s$, $^1$A′).

**Author Contributions:** Conceptualization, H.W.C., W.-J.C. and L.-S.W.; methodology, H.W.C. and L.-S.W.; formal analysis, H.W.C.; investigation, H.W.C., W.-J.C., G.S.K., D.-F.Y. and L.-S.W.; data curation, H.W.C. and W.-J.C.; writing—original draft preparation, H.W.C.; writing—review and editing, W.-J.C., G.S.K., D.-F.Y. and L.-S.W.; supervision, L.-S.W.; funding acquisition, L.-S.W. All authors have read and agreed to the published version of the manuscript.

**Funding:** This work was supported by the National Science Foundation under grant CHE-2053541.

**Data Availability Statement:** The data presented in this study are available from the corresponding authors upon reasonable request.

**Acknowledgments:** The authors thank the National Science Foundation for the support of this work through grant CHE-2053541.

**Conflicts of Interest:** The authors declare no conflict of interest.

## References

1. Lipscomb, W.N. The boranes and their relatives. *Science* **1977**, *196*, 1047–1055. [CrossRef]
2. Jemmis, E.D.; Prasad, D.L. Icosahedral $B_{12}$, macropolyhedral boranes, β-rhombohedral boron and boron-rich solids. *J. Solid State Chem.* **2006**, *179*, 2768–2774. [CrossRef]
3. Albert, B.; Hillebrecht, H. Boron: Elementary challenge for experimenters and theoreticians. *Angew. Chem. Int. Ed.* **2009**, *48*, 8640–8668. [CrossRef]
4. Oger, E.; Crawford, N.R.; Kelting, R.; Weis, P.; Kappes, M.M.; Ahlrichs, R. Boron cluster cations: Transition from planar to cylindrical structures. *Angew. Chem. Int. Ed.* **2007**, *46*, 8503–8506. [CrossRef]
5. Wang, L.S. Photoelectron spectroscopy of size-selected boron clusters: From planar structures to borophenes and borospherenes. *Int. Rev. Phys. Chem.* **2016**, *35*, 69–142. [CrossRef]
6. Jian, T.; Chen, X.; Li, S.-D.; Boldyrev, A.I.; Li, J.; Wang, L.S. Probing the structures and bonding of size-selected boron and doped-boron clusters. *Chem. Soc. Rev.* **2019**, *48*, 3550–3591. [CrossRef]
7. Pan, S.; Barroso, J.; Jalife, S.; Heine, T.; Asmis, K.R.; Merino, G. Fluxional boron clusters: From theory to reality. *Acc. Chem. Res.* **2019**, *52*, 2732–2744. [CrossRef]
8. Piazza, Z.A.; Hu, H.S.; Li, W.L.; Zhao, Y.F.; Li, J.; Wang, L.S. Planar hexagonal $B_{36}$ as a potential basis for extended single-atom layer boron sheets. *Nat. Commun.* **2014**, *5*, 3113. [CrossRef]
9. Mannix, A.J.; Zhou, X.-F.; Kiraly, B.; Wood, J.D.; Alducin, D.; Myers, B.D.; Liu, X.; Fisher, B.L.; Santiago, U.; Guest, J.R.; et al. Synthesis of borophenes: Anisotropic, two-dimensional boron polymorphs. *Science* **2015**, *350*, 1513–1516. [CrossRef]
10. Feng, B.; Zhang, J.; Zhong, Q.; Li, W.; Li, S.; Li, H.; Cheng, P.; Meng, S.; Chen, L.; Wu, K. Experimental realization of two-dimensional boron sheets. *Nat. Chem.* **2016**, *8*, 563–568. [CrossRef]
11. Xie, S.Y.; Wang, Y.; Li, X.B. Flat boron: A new cousin of graphene. *Adv. Mater.* **2019**, *31*, 1900392. [CrossRef]
12. Kaneti, Y.V.; Benu, D.P.; Xu, X.; Yuliarto, B.; Yamauchi, Y.; Golberg, D. Borophene: Two-dimensional boron monolayers: Synthesis, properties, and potential applications. *Chem. Rev.* **2022**, *122*, 1000–1051. [CrossRef]
13. Zhai, H.J.; Zhao, Y.F.; Li, W.L.; Chen, Q.; Bai, H.; Hu, H.S.; Piazza, Z.A.; Tian, W.J.; Lu, H.G.; Wu, Y.B.; et al. Observation of an all-boron fullerene. *Nat. Chem.* **2014**, *6*, 727–731. [CrossRef]
14. Romanescu, C.; Galeev, T.R.; Li, W.L.; Boldyrev, A.I.; Wang, L.S. Transition-metal-centered monocyclic boron wheel clusters (M© $B_n$): A new class of aromatic borometallic compounds. *Acc. Chem. Res.* **2013**, *46*, 350–358. [CrossRef]
15. Li, W.L.; Chen, X.; Jian, T.; Chen, T.T.; Li, J.; Wang, L.S. From planar boron clusters to borophenes and metalloborophenes. *Nat. Rev. Chem.* **2017**, *1*, 0071. [CrossRef]
16. Barroso, J.; Pan, S.; Merino, G. Structural transformations in boron clusters induced by metal doping. *Chem. Soc. Rev.* **2022**, *51*, 1098–1123. [CrossRef]
17. Lindsay, L.; Broido, D.; Reinecke, T. First-principles determination of ultrahigh thermal conductivity of boron arsenide: A competitor for diamond? *Phys. Rev. Lett.* **2013**, *111*, 025901. [CrossRef]
18. Tian, F.; Song, B.; Chen, X.; Ravichandran, N.K.; Lv, Y.; Chen, K.; Sullivan, S.; Kim, J.; Zhou, Y.; Liu, T.H. Unusual high thermal conductivity in boron arsenide bulk crystals. *Science* **2018**, *361*, 582–585. [CrossRef]
19. Shin, J.; Gamage, G.A.; Ding, Z.; Chen, K.; Tian, F.; Qian, X.; Zhou, J.; Lee, H.; Zhou, J.; Shi, L. High ambipolar mobility in cubic boron arsenide. *Science* **2022**, *377*, 437–440. [CrossRef]
20. Khairul, I.; Wang, Q.Q.; Jiang, Y.H.; Wang, C.; Naranmandura, H. Metabolism, toxicity and anticancer activities of arsenic compounds. *Oncotarget* **2017**, *8*, 23905. [CrossRef]
21. Byeon, E.; Kang, H.-M.; Yoon, C.; Lee, J.S. Toxicity mechanisms of arsenic compounds in aquatic organisms. *Aquat. Toxicol.* **2021**, *237*, 105901. [CrossRef] [PubMed]
22. Mohan, R. Green bismuth. *Nat. Chem.* **2010**, *2*, 336. [CrossRef] [PubMed]
23. Ramler, J.; Lichtenberg, C. Bismuth species in the coordination sphere of transition metals: Synthesis, bonding, coordination chemistry, and reactivity of molecular complexes. *Dalton Trans.* **2021**, *50*, 7120–7138. [CrossRef] [PubMed]

24. Zhang, Y.; Liu, Y.; Xu, Z.; Ye, H.; Yang, Z.; You, J.; Liu, M.; He, Y.; Kanatzidis, M.G.; Liu, S. Nucleation-controlled growth of superior lead-free perovskite $Cs_3Bi_2I_9$ single-crystals for high-performance X-ray detection. *Nat. Commun.* **2020**, *11*, 2304. [CrossRef] [PubMed]
25. Salvador, J.A.; Figueiredo, S.A.; Pinto, R.M.; Silvestre, S.M. Bismuth compounds in medicinal chemistry. *Future Med. Chem.* **2012**, *4*, 1495–1523. [CrossRef]
26. Madouri, D.; Ferhat, M. How do electronic properties of conventional III–V semiconductors hold for the III–V boron bismuth BBi compound? *Phys. Status Solidi B* **2005**, *242*, 2856–2863. [CrossRef]
27. Cui, S.; Feng, W.; Hu, H.; Feng, Z.; Wang, Y. First principles studies of phase stability, electronic and elastic properties in BBi compound. *Comput. Mater. Sci.* **2010**, *47*, 968–972. [CrossRef]
28. Bagci, S.; Yalcin, B.G. Structural, mechanical, electronic and optical properties of BBi, BP and their ternary alloys $BBi_{1-x}P_x$. *J. Phys. D Appl. Phys.* **2015**, *48*, 475304. [CrossRef]
29. Chen, W.J.; Kulichenko, M.; Choi, H.W.; Cavanagh, J.; Yuan, D.F.; Boldyrev, A.I.; Wang, L.S. Photoelectron spectroscopy of size-selected bismuth–boron clusters: $BiB_n^-$ ($n$ = 6–8). *J. Phys. Chem. A* **2021**, *125*, 6751–6760. [CrossRef]
30. Jian, T.; Cheung, L.F.; Chen, T.T.; Wang, L.S. Bismuth–boron multiple bonding in $BiB_2O^-$ and $Bi_2B^-$. *Angew. Chem. Int. Ed.* **2017**, *56*, 9551–9555. [CrossRef]
31. Cheung, L.F.; Czekner, J.; Kocheril, G.S.; Wang, L.S. High resolution photoelectron imaging of boron-bismuth binary clusters: $Bi_2B_n^-$ ($n$ = 2–4). *J. Chem. Phys.* **2019**, *150*, 064304. [CrossRef]
32. Gao, H.W.; Choi, H.W.; Hui, J.; Chen, W.J.; Kocheril, G.S.; Wang, L.S. On the electronic structure and spin-orbit coupling of BiB from photoelectron imaging of cryogenically-cooled $BiB^-$ anion. *J. Chem. Phys.* **2023**, *159*, 114301. [CrossRef]
33. Frisch, M.J.; Trucks, G.W.; Schlegel, H.B.; Scuseria, G.E.; Robb, M.A.; Cheeseman, J.R.; Scalmani, G.; Barone, V.; Mennucci, B.; Petersson, G.A.; et al. *Gaussian 09*; Gaussian Inc.: Wallingford, CT, USA, 2009.
34. Tao, J.; Perdew, J.P.; Staroverov, V.N.; Scuseria, G.E. Climbing the density functional ladder: Nonempirical meta–generalized gradient approximation designed for molecules and solids. *Phys. Rev. Lett.* **2003**, *91*, 146401. [CrossRef]
35. Peterson, K.A. Systematically convergent basis sets with relativistic pseudopotentials. I. Correlation consistent basis sets for the post-d group 13–15 elements. *J. Chem. Phys.* **2003**, *119*, 11099–11112. [CrossRef]
36. Kendall, R.A.; Dunning, T.H., Jr.; Harrison, R.J. Electron affinities of the first-row atoms revisited. Systematic basis sets and wave functions. *J. Chem. Phys.* **1992**, *96*, 6796–6806. [CrossRef]
37. Bauernschmitt, R.; Ahlrichs, R. Treatment of electronic excitations within the adiabatic approximation of time dependent density functional theory. *Chem. Phys. Lett.* **1996**, *256*, 454–464. [CrossRef]
38. Bannwarth, C.; Grimme, S. A simplified time-dependent density functional theory approach for electronic ultraviolet and circular dichroism spectra of very large molecules. *Comp. Theor. Chem.* **2014**, *1040–1041*, 45–53. [CrossRef]
39. Zubarev, D.Y.; Boldyrev, A.I. Developing paradigms of chemical bonding: Adaptive natural density partitioning. *Phys. Chem. Chem. Phys.* **2008**, *10*, 5207–5217. [CrossRef] [PubMed]
40. Zubarev, D.Y.; Boldyrev, A.I. Revealing intuitively assessable chemical bonding patterns in organic aromatic molecules via adaptive natural density partitioning. *J. Org. Chem.* **2008**, *73*, 9251–9258. [CrossRef]
41. Lu, T.; Chen, F. Multiwfn: A multifunctional wavefunction analyzer. *J. Comput. Chem.* **2012**, *33*, 580–592. [CrossRef]
42. Pyykkö, P. Relativistic effect in structural chemistry. *Chem. Rev.* **1988**, *88*, 563–594. [CrossRef]
43. Zubarev, D.Y.; Boldyrev, A.I. Comprehensive analysis of chemical bonding in boron clusters. *J. Comp. Chem.* **2007**, *28*, 251–268. [CrossRef] [PubMed]
44. Pyykkö, P. Additive covalent radii for single-, double-, and triple-bonded molecules and tetrahedrally bonded crystals: A summary. *J. Phys. Chem. A* **2015**, *119*, 2326–2337. [CrossRef] [PubMed]
45. Cheung, L.F.; Kocheril, G.S.; Czekner, J.; Wang, L.S. Observation of Möbius aromatic planar metallaborocycles. *J. Am. Chem. Soc.* **2020**, *142*, 3356–3360. [CrossRef] [PubMed]
46. Mauksch, M.; Tsogoeva, S.B. Demonstration of "Möbius" aromaticity in planar metallacycles. *Chem. Eur. J.* **2010**, *16*, 7843–7851. [CrossRef]